Comparative Studies on the Phase Stability, Electronic Structure, and Topology of the Charge Density in the Li_3XO_4 (X = P, As, V) Lithium Orthosalt Polymorphs

Christine Frayret,*,† Christian Masquelier,† Antoine Villesuzanne,‡ Mathieu Morcrette,† and Jean-Marie Tarascon†

LRCS-CNRS, Université de Picardie, 33, Rue Saint-Leu, 80039 Amiens Cedex, France, and ICMCB, CNRS, Université de Bordeaux 1, 87 Av. Dr. A. Schweitzer, 33608 Pessac Cedex, France

Received December 19, 2008. Revised Manuscript Received March 1, 2009

Density functional theory (DFT) calculations within the generalized gradient approximation (GGA) were performed to study phase transitions in lithium orthosalts Li_3XO_4 (X = P, As, V). The equilibrium crystal structure parameters and the total energies of the Li_3XO_4 polymorphs were calculated for the β- and γ-phases. The relative lattice stabilities of the two polymorphs were examined in the light of various peculiarities at atomic scale. The β-polymorph was systematically found to be the most stable one, agreeing well with experimental results. Using an all electron full potential method, we have investigated densities of states and the topology of charge density through the Bader's quantum theory of "atoms in molecules" (AIM) along with electrostatic energy density maps in order to evaluate factors governing the stability of each polymorph. Higher stability of the β-polymorph or differences in energy between β- and γ-phases according to the nature of X along with the experimental temperatures of phase transitions can be connected to several microscopic features, including differences in constraint within XO_4 tetrahedron or chemical bonding characteristics. This new approach can be applied to other phase stability studies, including the family of Li_2MSiO_4, which is of great interest for cathode materials in lithium batteries.

Introduction

The high stability of tetrahedral phosphate group $(PO_4)^{3-}$ is of primarily interest for applications of orthophosphate materials. Due to their high chemical and physical stability associated with the lithium mobility in the matrix, Li_3PO_4-based systems can be reliably used even in thin films for solid electrolyte materials within lithium battery setups.[1] In particular, LiPON electrolytes based on Li_3PO_4 have been envisaged for all-solid-state thin-film lithium batteries.[2] The strong structural stability provided by a tridimensional polyanionic skeleton made of $(PO_4)^{3-}$ groups, which constitutes the greatest advantage of these systems over layered transition metal oxides that lack their stability during Li intercalation/deintercalation, is also evidenced for other $(XO_4)^{n-}$ groups, including X = As, V or Cr, Mn.

Electrochemistry (ionic conductivity, capacity, or cycling) properties for these latter compounds have been observed as well.[3] One of the polymorphs of Li_3CrO_4 (β) can reversibly react with about 1 mol of Li ions per formula unit to give $Li_{3+x}CrO_4$ ($0 < x < 1$) with a discharge capacity of 196 mA h g^{-1}.[4] The possibility of exploiting multiple oxidation states for Mn (e.g., Mn^{3+} to Mn^{5+}) within positive electrodes in order to achieve high energy densities has been reported in some recent works.[5] According to these studies, extraction of Li from Li_3MnO_4 to form $LiMnO_4$ should occur at 3.4 V, while insertion of Li in the system to form Li_5MnO_4 could be possible at approximately 1.9 V for a total theoretical capacity of nearly 700 mA h g^{-1}. Mixed metal complexes, containing both $(MnO_4)^{n-}$ and $(VO_4)^{3-}$ oxyanions, are suggested in order to increase the electronic conductivity component, which is rather poor due to the salt-like structure of $(MnO_4)^{n-}$-based systems.

Due to their technological application, it is crucial to fully understand the polymorphism which characterizes lithium orthosalts. The crystal chemistry of Li_3PO_4, Li_3AsO_4, and Li_3VO_4 is similar, with isostructural low-temperature (β) and high-temperature (γ) phases for the three orthosalts. The structure is orthorhombic for both phases and the space group is $Pmn2_1$ for the low-temperature phase with $Z = 2$ and *Pnma* (*Pmnb* or *Pcmn* are sometimes used as well according to the setting choice) for the high-temperature one with $Z = 4$. Li and P cations are tetrahedrally coordinated by O anions in both phases. The β-form has the basic wurtzite structure in which one set of tetrahedral sites, T^+ or T^-, is fully occupied along with cation ordering (Figure 1a). A doubling of the unit cell along the *a*-axis (or along the *b*- or *c*-axis for *Pmnb* or *Pcmn* space groups, respectively) does occur

* To whom correspondence should be addressed. Tel: +33 322827586. Fax: +33 322827590. E-mail: christine.frayret@u-picardie.fr.
† Université de Picardie.
‡ Université de Bordeaux 1.

(1) Dudney. N. J. In *Lithium Batteries: Science and Technology*; Nazri, G.-A., Pistoia, G., Eds.; Kluwer Academic: Dordrecht, 2004; Chapter 20, pp 623−642.
(2) Lee, S.-H.; Liu, P.; Tracy, C. E. *Electrochem. Solid State Lett.* **2003**, *6*, A275.
(3) Mishra, K. M.; Lal, A. K.; Haque, F. Z. *Solid State Ionics* **2004**, *167*, 137.
(4) Garcia-Martin, S.; Robertson, A. D.; Dissanayake, M. A. K. L.; West, A. R. *Solid State Ionics* **1995**, *76*, 309.
(5) Saint, J. A.; Doeff, M. M.; Reed, J. *J. Power Sources* **2007**, *172*, 189.

10.1021/cm803429s CCC: $40.75
Published on Web 04/10/2009

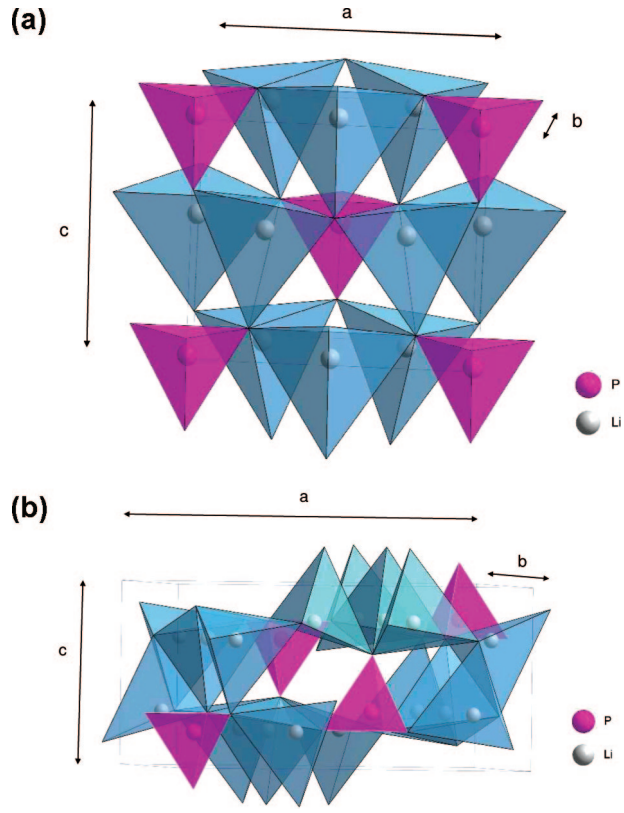

Figure 1. Crystallographic representation of the Li_3XO_4 β (a) and γ (b) polymorphs, showing the PO_4 (in pink) and LiO_4 (in blue) tetrahedra.

during the $\beta \rightarrow \gamma$ phase transition. The polymorphic phase transformation in Li_3PO_4 is related to Li and P cation redistributions within interstitial four-coordinated sites of the hexagonal closed-packed oxide layers: a diffusion of half of the P and Li cations in adjacent tetrahedra pointing along $[00\bar{1}]$ occurs upon the transition. The γ-phase also consists of hexagonal close-packed oxide layers, but these are more buckled in comparison with the β-structure (Figure 1b). Moreover, the cations are distributed over both sets of T^+ and T^- sites, leading LiO_4 tetrahedra to share some of their edges, while only corner-sharing is present in the β-structure.

Transition phases in Li_3XO_4 systems exhibit distinct features according to the nature of X. First, Li_3PO_4 differs from the isostructural compounds Li_3VO_4 and Li_3AsO_4 in its irreversible transformation at lower temperature (~400−600 °C for phosphate against reversible phase transformation at ~750 °C for arsenate or vanadate).[6,7] The β to γ transformation is also much more rapid for orthovanadate and arsenate than for Li_3PO_4. Moreover, temperature-controlled X-ray diffraction has demonstrated that of A_3XO_4 compounds, only Li_3PO_4 passes through the $\beta-\gamma$ inversion without the appearance of transitory phases, which arise spontaneously in Li_3VO_4 and Li_3AsO_4.

Beyond the direct interest of Li_3XO_4 materials, this study is intended to provide some basic information on the simplest systems related to these two structural types, in order to gain first insight into features characterizing polymorphism and in view of applying the same methodology to related compounds. A number of Li_3XO_4 derivative compounds have indeed been prepared, which have either one or both β- and γ-crystal structures. These more complex orthosalt derivatives include materials of general formula Li_2MXO_4, where M = Fe, Mg, Zn, Co and X = Si, Ge. Among this family, silicates such as Li_2FeSiO_4, Li_2MnSiO_4, and Li_2CoSiO_4 were envisaged as cathode materials in lithium batteries. Experimental works have proven that such materials can provide one electron per formula unit at average voltages of 3.1, 4.2, and 4.3 eV, respectively.[8−11] Iron silicate Li_2FeSiO_4 exhibits a theoretical energy capacity of 166 mA h g^{-1}.[12] The Li_2MSiO_4 family is built up from SiO_4, LiO_4, and MO_4 tetrahedral units and is closely related to Li_3PO_4 from the structural viewpoint. It is known to crystallize in several polymorphs (including $Pmn2_1$, $Pmnb$, $Pbn2_1$, and $P2_1/n$ space groups), which can be related to either the β- or the γ-form of Li_3PO_4.

In order to study the relative stability of the Li_3XO_4 polymorphs and the factors that contribute to the stability of each form, we undertook a series of first-principles calculations based on DFT and a topological analysis of the calculated charge density. The outline of the paper is as follows. In section 2, we detail the computational methods used in this study. In sections 3−8, we present the results and discussions of our geometry optimizations (section 3), calculations of total energies (section 4), densities of states (section 5), chemical bonding effects (section 6), atomic volumes (section 7) and electrostatic interactions (section 8). Rationalization of the polymorphism features in the light of the different effects studied at the atomic scale is proposed in section 9 while conclusions are presented in section 10.

2. Computational Methods

2.1. Structure Optimizations and Total Energy Calculations. Our structural optimizations have been performed by using first-principles density functional theory calculations as implemented in the Vienna Ab initio Simulation Program (VASP) package.[13−16] The computational scheme employed for this part of the study relies on a planewave basis set used for the valence electrons, while the core electrons and atom nuclei are represented using pseudopotentials. Therefore, only the valence electrons are treated explicitly. The projector augmented wave (PAW) method of Blöchl[17,18] was selected to treat electron−ion interactions, since it affords higher accuracy than the Vanderbilt ultrasoft pseudopotentials[19] and preserves the numerical advantages of pseudopotential codes, while retaining the physics of all-electron calculations. The generalized

(6) West, A. R.; Glasser, P. F. *J. Solid State Chem.* **1972**, *4*, 20.
(7) Reculeau, E.; Elfakir, A.; Quarton, M. *J. Solid State Chem.* **1989**, *79*, 205.
(8) Dominko, R.; Bele, M.; Gaberscek, M.; Meden, A.; Remskar, M.; Jamnik, J. *Electrochem. Commun.* **2006**, *8*, 217.
(9) Nyten, A.; Abouimrane, A.; Armand, M.; Gustafsson, T.; Thomas, J. O. *Electrochem. Commun.* **2005**, *7*, 156.
(10) Yang, Y.; Li, Y.; Gong, Z. IMLB 2006: International Meeting on Lithium Batteries; Biarritz, France, June 18−23, 2006, Abstract 210.
(11) Lyness, C.; Delobel, B.; Armstrong, A. R.; Bruce, P. *Chem. Commun.* **2007**, *46*, 4890.
(12) Quoirin, G. , Ph.D. Thesis, University of Picardie Jules Verne, Amiens, 2007.
(13) Kresse, G.; Hafner, J. *Phys. Rev. B* **1993**, *47*, RC558.
(14) Kresse, G.; Furthmüller, J. *J. Comput. Mater. Sci.* **1996**, *6*, 15.
(15) http://cms.mpi.univie.ac.at/vasp.
(16) Kresse, G.; Furthmüller, J. *Phys. Rev. B* **1996**, *54*, 11169.
(17) Blöchl, P. E. *Phys. Rev. B* **1994**, *50*, 17953.
(18) Kresse, G.; Joubert, D. *Phys. Rev. B* **1998**, *59*, 1758.
(19) Vanderbilt, D. *Phys. Rev. B* **1990**, *41*, 7892.

gradient approximation (GGA) exchange and correlation functional of Perdew−Burke−Ernzerhof (PBE) was used.[20] The kinetic energy cutoff was set up to 520 eV. A higher cutoff of 624 eV was also tested, giving no improvement in relative energies, with the difference of energy between β- and γ-polymorphs changed by less than 10^{-3} eV. Monkhorst−Pack meshes[21] of 4 × 4 × 5 and 2 × 4 × 5 points were used for sampling the Brillouin zones of β- and γ-polymorphs (in *Pnma* setting for the latter), respectively (for *Pcmn* setting of the γ-polymorph, a 5 × 4 × 2 mesh was used). A conjugate-gradient algorithm[22] was used for the structural minimization process and the remaining forces between ions after full optimization (atomic and cell coordinates) were less than 0.01 eV/Å. The electronic self-consistent field convergence criterion was 10^{-5} eV. Beyond structural information, total energies are also obtained after the full relaxation.

2.2. Calculations of Density of States and Topology of the Charge Density. Density of states (DOS) calculations have been performed at the level of DFT by using the full-potential linearized augmented plane waves method (FLAPW) as implemented in the Wien2k code.[23−25] The augmented plane wave plus local orbitals method (APW+lo) was used for valence states, and LAPW are used for the other states. The previously optimized structures were used as input, and the PBE functional was used for the exchange-correlation terms. The $R_{MT}K_{max}$ parameter, which is the product of the smallest muffin tin radius by the plane wave cutoff, was fixed to 7. Self-consistent cycles are achieved for 1000 and 500 k-points (i.e., 180 and 90 k-points samplings of the irreducible wedges of the Brillouin zones), for the β- and γ-polymorphs, respectively. Total energies are also provided through these calculations.

In addition, the topology of the electron density was investigated quantitatively. Such a terminology refers to several partition schemes by Mulliken,[26] Hirshfeld,[27] and Bader,[28−32] used for example to estimate atomic charges and thereby describe the ionicity or polarity of chemical bonds.

Here, Bader's or "atoms in molecules" (AIM) theory has been applied to the charge density calculated by the L/APW+lo method. An atom in a molecule or crystal is an open system, which is free to exchange charge and momentum with neighboring atoms; atomic boundaries are regions where the flux in the gradient vector field of the electron density vanishes, i.e. $\nabla\rho(r)\cdot n(r) = 0$, where $n(r)$ is the exterior normal vector to the surface of the region.

The Bader method is therefore based on the identification of zero flux surfaces around each nucleus, which correspond to density minima in interatomic space (vanishing density gradient). Zero flux surfaces (atomic envelopes) partition space into atomic basins, with well-defined, additive, and transferable properties, such as atomic volumes and populations. For example, the electron population in atomic basin Ω is given as $N(\Omega) = \int_\Omega \rho(r)\, dr$.

Table 1. Comparison of the Experimental and Optimized[a] Cell Parameters for the β-Li$_3$XO$_4$ Systems

	β-Li$_3$PO$_4$	β-Li$_3$AsO$_4$	β-Li$_3$VO$_4$
	Experimental		
ref	32	33	34
a (Å)	6.115	6.289	6.326
b (Å)	5.239	5.390	5.446
c (Å)	4.855	4.962	4.947
V (Å^3)	155.5	168.2	170.4
V/*Z* (Å^3)	77.8	84.1	85.2
	Calculated		
a (Å)	6.182 (+1.1%)	6.371 (+1.3%)	6.387 (+1.0%)
b (Å)	5.299 (+1.1%)	5.472 (+1.5%)	5.505 (+1.1%)
c (Å)	4.926 (+1.5%)	5.055 (+1.9%)	5.033 (+1.7%)
V (Å^3)	161.4 (+3.8%)	176.2 (+4.8%)	177.0 (+3.9%)
V/*Z* (Å^3)	80.7	88.1	88.5

[a] Discrepancies between the values are given in parentheses.

Table 2. Comparison of the Experimental and Optimized[a] Cell Parameters for the γ-Li$_3$XO$_4$ Systems[b]

	γ-Li$_3$PO$_4$	γ-Li$_3$AsO$_4$	γ-Li$_3$VO$_4$
	Experimental		
ref	35	36	37
a (Å)	10.490	10.908	4.970
b (Å)	6.120	6.369	6.400
c (Å)	4.927	5.149	10.900
V (Å^3)	316.3	357.7	346.7
V/*Z* (Å^3)	79.1	89.4	86.7
	Calculated		
a (Å)	10.628 (+1.3%)	10.945 (+0.3%)	5.166 (+3.9%)
b (Å)	6.181 (+1.0%)	6.384 (+0.2%)	6.394 (−0.1%)
c (Å)	5.005 (+1.6%)	5.169 (+0.4%)	10.984 (+0.8%)
V (Å^3)	328.8 (+4.0%)	361.2 (+1.0%)	362.8 (+4.6%)
V/*Z* (Å^3)	82.2	90.3	90.7

[a] Discrepancies between the values are given in parentheses. [b] For the γ-Li$_3$VO$_4$ compound, *Pcmn* space group setting has been selected.

In addition to the definition of atomic basins, the topology of electron density characterizes molecular or crystal structure in terms of critical points, where the gradient of the electron density vanishes, i.e. $\nabla\rho(r) = 0$. The accurate study of these critical points provides rigorous information especially on bonds and thus transforms the qualitative vision of chemical bonding based on electronegativity difference into a robust quantitative description and classification. The concepts underlying critical points are described in more detail in section 6.

3. Geometry Optimizations

The optimized cell parameters for the β- and γ-Li$_3$XO$_4$ systems are given in Tables 1 and 2, respectively. From a comparison with the experimental crystal structures,[33−38] it may be concluded that our DFT calculations allow a correct prediction of the cell parameters. The slight overestimation in values corresponds to a general trend traditionally observed in calculations based on GGA exchange and correlation potentials. Volume augmentation lies between 3.8 and 4.8%, except for γ-Li$_3$AsO$_4$, in which the value is lower (+1.0%). An anisotropic behavior of the lattice parameters evolution

(20) Perdew, J. P.; Burke, K.; Ernzerhof, M. *Phys. Rev. Lett.* **1996**, *77*, 3865.
(21) Monkhorst, H. J.; Pack, J. D. *Phys. Rev. B* **1977**, *13*, 5188.
(22) Feynman, R. P. *Phys. Rev.* **1939**, *56*, 340.
(23) Blaha, P.; Schwarz, K.; Madsen, G. K. H., Kvasnicka, D.; Luitz, J. *An augmented plane wave plus local orbitals program for calculating crystal properties*; Vienna University of Technology: Vienna, Austria, 2001; ISBN 3-9501031-1-2.
(24) Schwarz, K.; Blaha, P.; Madsen, G. K. H. *Comput. Phys. Commun.* **2002**, *147*, 71.
(25) WIEN2k: http://www.wien2k.at.
(26) Mulliken, R. S. *J. Chem. Phys.* **1955**, *23*, 1833.
(27) Hirschfeld, F. L. *Theor. Chim. Acta* **1977**, *44*, 129.
(28) Bader, R. F. W. *Atoms in Molecules: A Quantum Theory*; Clarenden Press: Oxford, 1994.
(29) Bader, R. F. W. *Chem. Rev.* **1991**, *91*, 893.
(30) Bader, R. F. W. *J. Phys. Chem. A* **1998**, *102*, 7314.
(31) Pendás, A. M.; Costales, A.; Luaña, V. *Phys. Rev. B* **1997**, *55*, 4275.
(32) Aray, Y.; Rodriguez, J.; Vega, D. *Comput. Phys. Commun.* **2002**, *143*, 199.
(33) Keffer, C.; Mighell, A. D.; Mauer, F.; Swanson, H.; Block, S. *Inorg. Chem.* **1967**, *6*, 119.
(34) Elfakir, A.; Wallez, G.; Quarton, M.; Pannetier, J. *Phase Transition* **1993**, *45*, 281.
(35) Shannon, R. D.; Calvo, C. *J. Solid State Chem.* **1973**, *6*, 538.
(36) Yakubovich, O. V.; Urosova, V. S. *Kristallografiya* **1997**, *42*, 301.
(37) Abrahams, I.; Bruce, P. G.; David, W. I. F.; West, A. R. *J. Solid State Chem.* **1994**, *110*, 243.
(38) Blasse, G. *Z. Anorg. Allg. Chem.* **1964**, *331*, 44.

Table 3. List of Bond Lengths (in Å) for the Experimental and Optimized Structures of the β-Li_3XO_4 Systems

crystal	X−O_{min}	X−O_{max}	⟨X−O⟩
β-Li_3PO_4			
expt[32]	1.540	1.549	1.545
calc	1.558	1.562	1.561
β-Li_3AsO_4			
expt[33]	1.670	1.725	1.689
calc	1.726	1.728	1.725
β-Li_3VO_4			
expt[34]	1.714	1.721	1.719
calc	1.731	1.739	1.736

Table 4. List of Bond Lengths (in Å) for the Experimental and Optimized Structures of the γ-Li_3XO_4 Systems

crystal	X−O_{min}	X−O_{max}	⟨X−O⟩
γ-Li_3PO_4			
expt[35]	1.542	1.545	1.544
calc	1.556	1.561	1.559
γ-Li_3AsO_4			
expt[36]	1.671	1.700	1.673
calc	1.720	1.730	1.727
γ-Li_3VO_4			
expt[37]	1.599	1.605	1.588
calc	1.730	1.740	1.736

may be noticed. For the whole of β- Li_3XO_4 systems, the highest increase is found for the *c* parameter. This situation is maintained for γ-Li_3PO_4, while a large discrepancy is observed for the *a* parameter in γ-Li_3VO_4. In γ-Li_3AsO_4, the increase in lattice parameter is roughly isotropic and of small extent.

For the β-polymorph, an increase in lattice volume is found by passing from P to As and V, in agreement with experiment. Such a sequence is maintained for the γ-phase, while Li_3AsO_4 seems to be characterized experimentally by a higher volume than γ-Li_3VO_4. It must be underlined that both experimental and calculated lattice volumes (*V*/*Z*) exhibit higher increase from the β- to the γ-form, when X = V and As than for X = P.

Bond lengths for the β- and γ-Li_3XO_4 systems are displayed in Tables 3 and 4, respectively. As expected, a systematic overestimation is observed. For both β- and γ-polymorphs, a noticeable increase in bond lengths is found by passing from P to As or V, whereas a similar order of magnitude is observed for arsenate and vanadate salts, in agreement with experiment. However, those tendencies cannot be directly exploited in themselves in view of comparing and interpreting covalency trends in those compounds, since ionic radii are not equal. In particular, ionic radius in 4-fold coordination of P ($r_{P^{5+}} = 0.17$ Å) is markedly smaller than those of As and V ($r_{As^{5+}} = 0.34$ Å, $r_{V^{5+}} = 0.36$ Å).[39] The very slight increase in average values in bond lengths from β- to γ-phase, observed experimentally, is confirmed by calculations.

4. Total Energies

The results for the relative internal energy differences for the β- and γ-polymorphs are summarized in Table 5. The β- structure is systematically found to be more stable than the γ-form. These results are consistent with experiment, for which the β-form is the low temperature one[40] and with previous theoretical works.[41,42]

Table 5. Internal Energies Differences (in eV/formula unit) between the Two Crystalline Forms of Li_3XO_4 Relative to the Most Stable β-Phase

	generalized gradient approximation	
crystal	PAW	APW+lo
Li_3PO_4	0.008	0.013
Li_3VO_4	0.023	0.020
Li_3AsO_4	0.027	0.029

The table shows that the two independent computational methods give consistent results. The relative differences in energy between the two crystallographic phases are very small (as expected from other energetics studies of various crystalline polymorphs), with $\Delta E/Z$ of less than 0.03 eV. However, the higher stability of the β-form relative to the γ one continuously increases upon passing from P (∼0.01 eV/formula unit) to V and As, with double (∼0.02 eV/fu) and triple (∼0.03 eV/fu) magnitude in stability found for the two last compounds, respectively. Since we do not know of experimental measurements of these relative energies, we are limited to considering these DFT calculation values (which are very small as already outlined) in order to account for the relative stability between β- and γ-polymorphs as a function of X. It would be interesting to compare these data with the relative stability of the polymorphs determined experimentally, through calorimetry measurements, on the basis of the estimation of their enthalpies of formation.

Relative incidence of the various factors likely to influence this phase transition at the atomic scale in Li_3PO_4, Li_3AsO_4, and Li_3VO_4 will be presented in detail in the next sections. The aim of this work is clearly to find explanations for the systematic highest stability of the β-polymorph and to correlate the energy differences varying with the nature of X to one or several microscopic features.

5. Density of States

Parts a and b of Figure 2 show the projected densities of state (DOS) for the β- and γ-polymorphs of the Li_3XO_4 materials, respectively.

5.1. Li_3PO_4. Li_3PO_4 exhibits the typical behavior of a large band gap insulator. The two polymorphs are characterized by very similar profiles with band gaps around 6 eV (6 and 5.9 eV for β- and γ-forms), to be compared with reported optical gaps of ∼7−8 eV.[43] Yet, bandwidths for the β-Li_3PO_4 are slightly smaller than those of the γ-phase (see insets). Another distinction appears for states located at the very top of the valence band, for which a strong localization on the O 2p orbital is found in the β-form, whereas those electrons are strongly delocalized on O, Li, and P orbitals in the γ-phase. This effect might originate from the lower symmetry of the HT phase.

(39) Shannon, R. D.; Prewitt, C. T. *Acta Crystallogr. A* **1976**, *32*, 751.
(40) Rojas, R. M.; de Vidales, J. L. M.; Delgado, A.; Sinisterra, J. V. *J. Solid State Chem.* **1993**, *106*, 237.
(41) Du, Y. A.; Holzwarth, N. A. W. *Phys. Rev. B* **2007**, *76*, 174302.
(42) Arroyo de Dompablo, M. E.; Dominko, R.; Gallardo-Amores, J. M.; Dupont, L.; Mali, G.; Ehrenberg, H.; Jamnik, J.; Morán, E. *Chem. Mater.* **2008**, *20*, 5574.
(43) Harbach, F.; Fischer, F. *Phys. Status Solidi B* **1974**, *66*, 237.

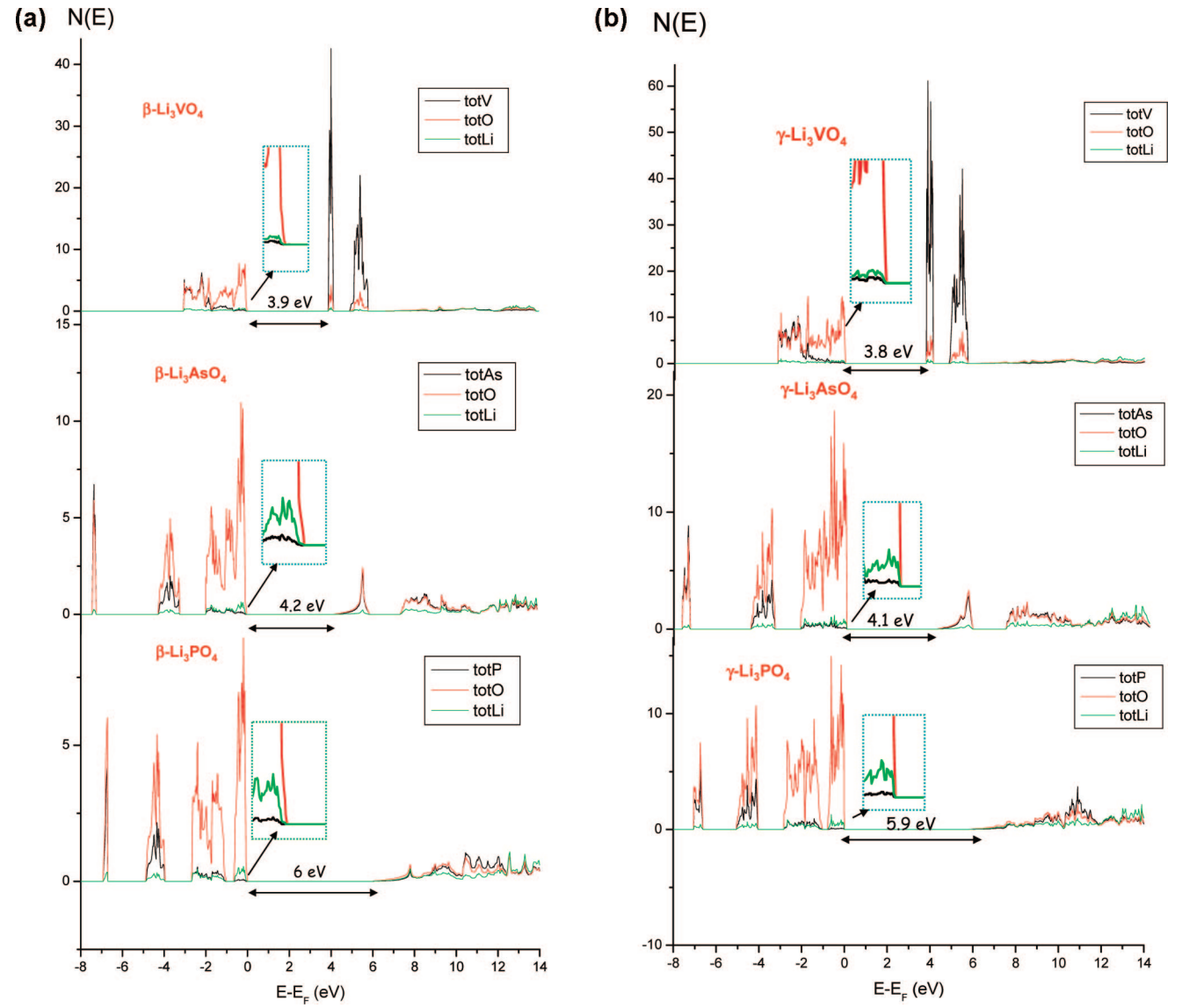

Figure 2. Partial densities of states for Li_3XO_4 (X = P, As, V) in the β (a) and γ (b) crystalline form.

For both forms, the valence band (VB) has strong O 2p character, low contribution of Li 2s states, and is clearly separated in four blocks. These bands correspond to the strongly covalently bonded PO_4 tetrahedron. The lowest energy part (near −7 eV) corresponds to the O 2pσ bonds with the P 3s states, while the upper portion (near −5 eV) is related to O 2pσ bonds with the P 3p states. The VB in the range -3 eV $< E < -1$ eV is characterized by a small and nearly identical hybridization with P pπ states and Li 2s. The states at the top of the valence band, in the range -1 eV $< E < 0$ eV, are characterized by a small hybridization as well, with slight contribution of Li 2s states and negligible admixture of P ones. The conduction band (CB) is mainly composed of P 3s and O 2p orbitals.

5.2. Li_3AsO_4. The basic features of the VB remain when As is substituted for P. Just below −7 eV, bands correspond to the O 2pσ bonds with the As 3s states, and O 2pσ bonds with As 3p states are found around −4 eV. Upper valence states exhibit low hybridization, although it seems to be higher in the case of the γ-polymorph, due to the higher splitting aspect of the band. The CB in the range 4 eV $< E <$ 6 eV is characterized by strong O 2p and As 4s character, while in the range 7 eV $< E <$ 9 eV, strong admixture of O 2p and As 4p is evidenced. Apart from the slight distinction already observed between both polymorphs, we notice, similarly to the lithium orthophosphate, that a prevailing localization of electrons on the O 2p orbitals exists for the β-form, whereas these electrons are delocalized on the orbitals belonging to the three atoms for the γ-form (see insets).

The calculated band gaps are respectively of 4.2 and 4.1 eV for the β- and γ-polymorphs. Unfortunately, no experimental value of gap is available for Li_3AsO_4 to compare with our calculated data.

5.3. Li_3VO_4. The two Li_3VO_4 polymorphs once more exhibit very close DOS behavior, with band gaps of 3.8−3.9 eV for the γ- and β-forms, respectively, in very good agreement with the experimental optical gap of ∼3.7 eV.[44] As already observed in phosphate and arsenate compounds, the main difference between both polymorphs originates from a strong localization on the O 2p orbital at the very top of

(44) Sakata, S.; Nagoshi, Y.; Nii, H.; Ueda, N.; Kawazoe, H. *J. Appl. Phys.* **1996**, *80*, 3668.

Table 6. Electron Population and Atomic Charges for the Two Polymorphs of Li_3XO_4 Calculated by the Bader AIM Approach within the Wien2k Implementation, Electron Population Evolution with Respect to the Most Stable Phase, and Atomic Charges

			N_{el}			
X	atom	Z	β	γ	$\Delta N_{el}/N_{el\ \beta}$ (%)	charge (β, γ)
P	O	8	9.62	9.62	0	–1.62
	P	15	11.18	11.18	0	+3.82
	Li	3	2.11	2.11	0	+0.89
As	O	8	9.35	9.35	0	–1.35
	As	33	30.27	30.26	0.03	+2.73(4)
	Li	3	2.10	2.11	0.5	+0.89(90)
V	O	8	9.20(21)	9.21	0	–1.20(1)
	V	23	20.84	20.84	0	+2.16
	Li	3	2.11	2.11	0	+0.89

the VB in the β-form, whereas a high delocalization on O, Li, and V orbitals characterizes the γ-phase (see insets). The extent of both VB and CB is smaller in Li_3VO_4 than in Li_3PO_4 or Li_3AsO_4. At the bottom of the VB, in the range -4.4 eV $< E <$ 2.2 eV, a high hybridization between O 2p and V 3d is noticed, whereas in the upper part of the VB the predominant character of O 2p along with small Li 2s contribution are observed. The CB of vanadate materials is composed of V 3d, O 2p, and Li 2s and has strong d character owing to the larger contribution of V 3d orbitals than the others. In particular, the first conduction band has mostly metal d-character.

We shall recall here that band gaps are usually underestimated in DFT calculations with respect to the measured values, but their relative values for different phases and materials are usually meaningful. In β- and γ-forms, we have found that the calculated band gaps for Li_3XO_4 increase from X = V or As to X = P, with quasi-inexistent difference between Li_3VO_4 and Li_3AsO_4. This constitutes an indication of the higher ionic character of bonding in the phosphate material, characterized by a larger gap.

6. Chemical Bonding Effects

6.1. Atomic Charges. Electron population and corresponding atomic charges obtained through electron density partitioning within AIM approach are summarized in Table 6. As expected, due to the iono-covalent character of bonds, atomic electron populations lie in between those expected for purely covalent or ionic bonds.

For all the Li_3XO_4 polymorphs, the Bader charges for oxygen range from -1.21 to -1.62, those of lithium are systematically equal to $+0.89$ to $+0.90$, while those of X lie between $+2.16$ and $+3.82$. Whatever the orthosalt, the charge of the lithium atom is very close to the nominal $+1$ value. For Li_3PO_4, we can mention that the values of the oxygen atomic charges are on the same order of magnitude as those found by Du and Corrales for lithium silicate crystals.[45] According to the complete set of data, no differences are found between inequivalent positions. Therefore, charges are indicated by atom nature only. Moreover, nearly no (or rather low) difference in charge is found between β- and γ-polymorphs, whatever the nature of X.

By passing from X = V or As to P, a clear increase in ionic character is evidenced, due to the increase in both O and X atomic charges (in absolute values). This result is in agreement with observations on DOS discussed in the previous part. However, deeper insight is gained through atomic charges, since more or less ionic character can now be exclusively ascribed to the X−O bonding feature differences, given that no discrepancy between Li−O bonds is found among Li_3PO_4, Li_3AsO_4, and Li_3VO_4.

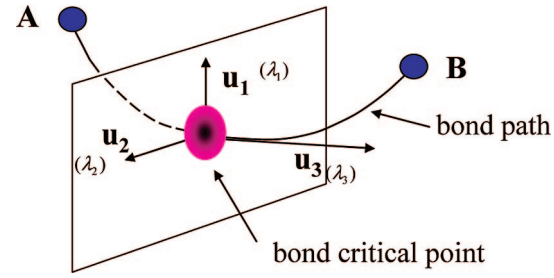

Figure 3. Representation of bond path between two atoms (A and B) showing the directions associated with perpendicular (λ_1, λ_2) and parallel (λ_3) curvatures at the bond critical point.

Concerning the comparison between the arsenate and the vanadate, higher charge transfer between M and O seems to occur in the former, whereas very similar band gaps were obtained for both materials. With respect to this, we shall recall that information gained from atomic charges is only qualitative and should not be considered to afford a complete vision of the iono-covalent character of the different bonds, as demonstrated by recent works.[45−47] Such precise and quantitative differentiation in chemical bonding can be gained either by population analysis methods issued from electron deformation density, rather than from total electron density,[45] or from the critical points analysis, which is discussed hereafter.

Yet, as far as the phosphate salt is concerned, the difference in atomic charges seems to be sufficiently unambiguous to attempt to correlate total energies or phase transitions features and ionic character of bonds; this then should be confronted to peculiarities afforded by critical points analysis, presented in the next part.

6.2. Bond Critical Points. A critical point (CP) in the charge density is a point where the gradient of a charge density vanishes, i.e., where $\nabla\rho(r) = 0$. It is labeled according to its rank (number of nonzero values of the Hessian matrix $H_{ij} = \partial^2\rho(r)/(\partial x_i \partial y_j)$ and its signature (excess number of positive over negative eigenvalues); (3, −3), (3, +3), and (3, −1) correspond, respectively, to maxima, minima, and saddle points. Thus, a (3, −1) critical point is referred to be a bond critical point. We can characterize each bond critical point (BCP) by the main curvatures of the charge density corresponding to the three eigenvalues (λ_1, λ_2, and λ_3) of the Hessian matrix.

For a bond critical point (BCP), the two curvatures calculated in the directions perpendicular to the bond (λ_1 and λ_2) are negative, while the curvature parallel to the bond path, λ_3, is positive (Figure 3). $|\lambda_1|$ and $|\lambda_2|$ denote the curvatures measured in two mutually perpendicular directions perpen-

(45) Du, J.; Corrales, L. R. *J. Phys. Chem. B* **2006**, *110*, 22346.
(46) Davidson, E. R.; Chakravorty, S. *Theor. Chim. Acta* **1992**, *83*, 319.
(47) Segall, M. D.; Pickard, C. J.; Shah, R.; Payne, M. C. *Mol. Phys.* **1996**, *89*, 571.

Table 7. Bond Length (l_e in Å, rounded to two decimal places), Distance from the Bond Critical Point to Atom 1 (d_1 in Å) and Atom 2 (d_2 in Å), Bond Path Length (l_b in Å), Electron Density (ρ in e Å^{-3}), Eigenvalues of Hessian and Laplacian [λ_i ($i = 1-3$), $\nabla^2\rho Z$ in e Å^{-5}] of ρ, and the Ratio $|\lambda_1|/\lambda_3$ at the Bond Critical Points in β-Li_3XO_4 Crystals

X	bond	l_e	d_1 (X/Li−CP)	d_2 (O−CP)	l_b	ρ	λ_1	λ_2	λ_3	$\nabla^2\rho$	$\lvert\lambda_1\rvert/\lambda_3$
P	P−O_1	1.56	1.19	1.77	2.96	0.21	−0.37	−0.37	1.43	0.69	0.26
	P−O_2	1.56	1.19	1.76	2.95	0.21	−0.37	−0.37	1.44	0.70	0.26
	P−O_3	1.56	1.18	1.76	2.94	0.21	−0.38	−0.38	1.46	0.70	0.26
	Li−O_1	1.99	1.43	2.33	3.76	0.03	−0.04	−0.04	0.25	0.17	0.16
	Li−O_2	1.99	1.42	2.32	3.74	0.03	−0.04	−0.04	0.24	0.16	0.17
	Li−O_3	1.96	1.40	2.28	3.68	0.03	−0.04	−0.04	0.27	0.19	0.15
As	As−O_1	1.73	1.58	1.69	3.27	0.18	−0.22	−0.22	0.80	0.36	0.28
	As−O_2	1.73	1.58	1.68	3.26	0.18	−0.23	−0.23	0.81	0.35	0.28
	As−O_3	1.73	1.58	1.68	3.26	0.18	−0.22	−0.22	0.81	0.37	0.27
	Li−O_1	2.00	1.44	2.35	3.79	0.03	−0.04	−0.04	0.23	0.15	0.17
	Li−O_2	2.00	1.44	2.34	3.78	0.03	−0.04	−0.04	0.24	0.16	0.17
	Li−O_3	1.97	1.42	2.31	3.73	0.03	−0.04	−0.04	0.26	0.18	0.15
V	V−O_1	1.74	1.58	1.71	3.29	0.18	−0.25	−0.25	1.10	0.60	0.23
	V−O_2	1.74	1.57	1.71	3.28	0.18	−0.25	−0.25	1.10	0.60	0.23
	V−O_3	1.73	1.56	1.71	3.27	0.18	−0.26	−0.26	1.11	0.59	0.23
	Li−O_1	2.00	1.44	2.33	3.77	0.03	−0.04	−0.04	0.23	0.15	0.17
	Li−O_2	2.00	1.44	2.34	3.78	0.03	−0.04	−0.04	0.23	0.15	0.17
	V−O_3	1.98	1.43	2.31	3.74	0.03	−0.04	−0.04	0.25	0.17	0.16

dicular to the bond path and are linked to the local charge concentration in the surface at this BCP. λ_3 is related to the parallel expansion of $\rho(r)$, which leads to its depletion away from BCP. Thus, the formation of an interatomic surface and of a chemical bond is the result of a competition between the perpendicular compression and parallel expansion of the electron density.

The ratio between the perpendicular and parallel curvatures $|\lambda_1|/\lambda_3$ together with the Laplacian [the trace of the Hessian of $\rho(r_c)$, $\nabla^2\rho(r_c) = \lambda_1 + \lambda_2 + \lambda_3$] provides quantitative information, suitable for both classification and comparison of chemical bonding. The $|\lambda_1|/\lambda_3$ ratio is a measure of bond directionality. An inverse ratio ($\lambda_3/|\lambda_1|$) close to zero indicates a high directional character of the chemical bond, as in shared-shell bonds. Large values of $\lambda_3/|\lambda_1|$ are typical of closed-shell interactions. In regions where the Laplacian $\nabla^2\rho$ is negative, the electron density is locally greater than the average value in the immediate vicinity of r; $\rho(r)$ is thus indicative of a local concentration.

For regions where $\nabla^2\rho$ is positive, the situation is the reverse: the electron density is locally less than the average value in the immediate vicinity of r, and $\rho(r)$ is said to be locally depleted. For a closed-shell interaction, $\nabla^2\rho$ is pictured as being positive over much of the internuclear region including r_c but negative in the region of the valence shell of the more electronegative atom, where the electron density is locally concentrated. According to the topology properties at BCPs, two kinds of interatomic interactions can thus be observed: shared and closed-shell interactions.[28] For a BCP of shared interaction, corresponding to covalent bonds, the Laplacian is negative at r_c, the electron density is larger (order 1 in e Å^{-3}), and the ratio $|\lambda_1|/\lambda_3$ is larger than unity. The closed-shell interaction is characterized by a positive Laplacian at r_c, lower electron density, and a smaller $|\lambda_1|/\lambda_3$ ratio at the BCPs. Ionic, hydrogen, and van der Waals bonds fall in this category. The connection between the topology of the electron density and the chemical and structural stability of isolated molecules is well-known: the value of the electron density at the critical point is closely related to the stability of the molecule.[48,49] In a similar way, Aray et al.[50] established that the electron density at the critical point in fcc transition metals is essentially proportional to the cohesion energy and therefore provides a measure of the bond strength in the case of crystals.

The inequivalent BCPs, denoted by the atoms they connect, are listed in Tables 7 and 8 for β- and γ-polymorphs, respectively. The bond length (l_e), distance from the bond critical point to atom 1 (X/Li) (d_1) and atom 2 (O) (d_2), bond path length (l_b), electron density, eigenvalues of Hessian and Laplacian of ρ (sum of eigenvalues), and the ratio $|\lambda_1|/\lambda_3$ are given. For the sake of simplicity, Tables 7 and 8 only present the results for one Li atom (Li1), the results for the second lithium atom being very similar. BCP data clearly demonstrate that all the bonding interactions in Li_3XO_4 polymorphs belong to closed-shell interaction (except one Li−O bond in γ-Li_3AsO_4), since the Laplacian of the charge density is positive with a small magnitude, the electron density at r_c is small, and the $|\lambda_1|/\lambda_3$ ratio is smaller than unity (i.e., λ_3 dominates). This is in accordance with the large charge transfer between the atoms for these compounds.

Apart from this general classification scheme, indicating the major ionic character of bonding, the value of the electron density distribution at the bond critical point and the length of a given bond are reliable measures of a bonded interaction: the greater the accumulation of the electron density and the shorter the bond, the greater its shared (covalent) interaction. It is noticed, in both β- and γ-forms, that P−O bonds are shorter and have higher electron density at BCP than V−O and As−O bonds. More precisely, with decreasing X−O bond length by passing from Li_3AsO_4 or Li_3VO_4 to Li_3PO_4 phases, four main features are observed: (1) the value of the electron density ρ at r_c along the bond path increases, (2) the curvatures, $|\lambda_1|$ and $|\lambda_2|$, of $\rho(r_c)$ perpendicular to the bond path both increase, (3) the curvature, λ_3, of $\rho(r_c)$ along the bond path increases, and (4) the Laplacian of $\rho(r_c)$, $\nabla^2\rho(r_c)$, increases. Thus, as the bond shortens, there is a progressive

(48) Bader, R. F. W.; Essen, H. *J. Chem. Phys.* **1984**, *80*, 1943.
(49) Knop, O.; Boyd, R. J.; Choi, S. C. *J. Am. Chem. Soc.* **1988**, *110*, 7299.
(50) Aray, Y.; Rodriguez, J.; Vega, D. *J. Phys. Chem. B* **2000**, *104*, 4608.

Table 8. Bond Length (l_e in Å, rounded to two decimal places), Distance from the Bond Critical Point to Atom 1 (d_1 in Å) and Atom 2 (d_2 in Å), Bond Path Length (l_b in Å) Electron Density (ρ in e Å^{-3}), Eigenvalues of Hessian and Laplacian [λ_i ($i = 1-3$), $\nabla^2\rho Z$ in e Å^{-5}] of ρ and the Ratio $|\lambda_1|/\lambda_3$ at the Bond Critical Points in γ-Li_3XO_4 Crystals

X	bond	l_e	d_1 (X/Li−CP)	d_2 (O−CP)	l_b	ρ	λ_1	λ_2	λ_3	$\nabla^2\rho$	$\lvert\lambda_1\rvert/\lambda_3$
P	P−O_1	1.56	1.19	1.76	2.95	0.21	−0.37	−0.37	1.44	0.70	0.26
	P−O_2	1.56	1.18	1.76	2.94	0.21	−0.38	−0.38	1.48	0.72	0.26
	P−O_3	1.56	1.19	1.76	2.95	0.21	−0.37	−0.37	1.44	0.70	0.26
	Li−O_1	2.00	1.42	2.31	3.73	0.03	−0.04	−0.04	0.26	0.18	0.15
	Li−O_2	1.98	1.42	2.31	3.73	0.03	−0.04	−0.04	0.25	0.17	0.16
	Li−O_3	1.95	1.41	2.29	3.70	0.03	−0.04	−0.04	0.27	0.19	0.15
As	As−O_1	1.73	1.58	1.68	3.26	0.18	−0.22	−0.22	0.81	0.37	0.28
	As−O_2	1.72	1.57	1.68	3.25	0.18	−0.23	−0.23	0.82	0.36	0.28
	As−O_3	1.73	1.58	1.69	3.27	0.18	−0.22	−0.22	0.80	0.36	0.28
	Li−O_1	2.01	1.43	2.34	3.77	0.03	−0.04	−0.04	0.24	0.16	0.17
	Li−O_2	1.98	2.05	2.13	4.18	0.10	−0.11	−0.11	0.11	–0.11	1.00
	Li−O_3	1.98	1.42	2.31	3.73	0.03	−0.04	−0.04	0.26	0.18	0.15
V	V−O_1	1.74	1.57	1.71	3.28	0.18	−0.25	−0.25	1.10	0.60	0.23
	V−O_2	1.73	1.56	1.70	3.26	0.18	−0.26	−0.26	1.13	0.61	0.23
	V−O_3	1.74	1.58	1.71	3.29	0.18	−0.25	−0.25	1.08	0.58	0.23
	Li−O_1	2.01	1.43	2.31	3.74	0.03	−0.04	−0.04	0.25	0.17	0.16
	Li−O_2	1.99	1.43	2.32	3.75	0.03	−0.04	−0.04	0.24	0.16	0.17
	V−O_3	1.98	1.43	2.31	3.74	0.03	−0.04	−0.04	0.25	0.17	0.16

buildup of electron density at r_c with a concomitant local concentration of the electron density both perpendicular to the path of the bond and in the direction parallel to the path away from r_c toward X and O (Figure 4). These effects are also accompanied with a clear migration of r_c toward the X cation. Such observations are in agreement with the higher directional character of the P−O bond (higher $|\lambda_1|/\lambda_3$ ratio) and might be ascribed to a weaker V−O or As−O bonding relative to P−O bonding. This bonding effect could give less stabilizing component for Li_3VO_4 and Li_3AsO_4, whereas, on the other hand, the distinction between the two polymorphs is quasi-inexistent for all Li_3XO_4 compounds.

By comparing Li_3VO_4 and Li_3AsO_4, it is straightforward to see that X−O BCPs are characterized by very similar features in both chemical bond length and electron density at r_c (Figure 4). This is consistent with very similar band gaps observed for both materials. Therefore, atomic charges comparison is not precise enough to account for the difference in chemical bonding properties between these two compounds. From the BCP study, the only difference between both materials originates from a slightly lower $|\lambda_1|$ value and a concomitant more notable decrease in λ_3 value, which depreciates as a whole the Laplacian value for Li_3AsO_4.

Concerning Li−O bonds, the longer bond distance and the very low value of ρ at r_c are indicative of a very high ionic character, which is consistent with a notably lower $|\lambda_1|/\lambda_3$ ratio as compared with X−O bonds. We can note that, for γ-Li_3AsO_4, one of the bonds (Li−O2) is characterized by a shared interaction (negative value of Laplacian, $|\lambda_1|/\lambda_3$ ratio equal to unity) and is therefore somewhat devoid of ionic character (very low value of λ_3). This is a strong departure of the γ-form of Li_3AsO_4, which is the only one for which such differentiation between both polymorphs does occur. Such effect should have an incidence on the stability of the γ-polymorph of Li_3AsO_4 and should contribute to its destabilization, in comparison with β-form. Such additional stabilizing effect for the β-form of Li_3AsO_4 contributes to the enhancement in total energy difference between the two polymorphs for this compound.

For all the bonds, the bond path length (l_b = sum of d_1 and d_2) is larger than the bond length (l_e). This observation demonstrates that the bond between the two atoms (X/O or Li/O) is not straight but bent.

7. Atomic Volumes

Atomic basins issued from AIM analysis are presented in Table 9 in connection with X−O interatomic distances evolution for PO_4 polyhedra. As expected, the whole crystal volume is dominated by O atoms.[51−53] As a whole, atomic basins follow ionic radii trends in terms of relative atomic sizes, with values of nearly 3 and 8 Å^3 for P and As or V ions, respectively, while ionic radius is also much lower for P ion ($r_{P^{5+}} = 0.17$ Å) and roughly of the same for As and V ions ($r_{As^{5+}} = 0.34$ Å, $r_{V^{5+}} = 0.36$ Å) in four-coordination.[39] This effect is well-illustrated in Figure 5a,b, showing atomic envelopes of the X cation and two neighboring O in orthophosphate and arsenate, respectively. On the other hand, visualization of atomic envelopes demonstrates that X atom shape is closely related to its coordination number (4): basins have tetrahedral form (Figure 5a,b). Due to the smaller size of phosphorus cation, it is more suited for four-coordination as compared with vanadium or arsenate cations.

Upon β to γ transformation, we can observe that the XO_4 tetrahedron (made of two O_1, one O_2, and one O_3) increases in volume by ~2 Å^3 for P and 3 Å^3 for V, respectively, while the one characterizing the orthoarsenate is unchanged. Contrary to atomic charges, for which no evolution is found between β- and γ-forms, a clear differentiation among the two polymorphs is evidenced for atomic volumes. This tends to indicate that a gap does exist between all lithium orthosalts from the viewpoint of Born-type short-range repulsive energy component. Indeed, if distances become too short, local interpenetration of electron clouds is generated, resulting in sterical hindrance and unfavorable short-range interactions.

(51) Oganov, A. R.; Gillan, M. J.; Price, G. D. *Phys. Rev. B* **2005**, *71*, 064104.
(52) Frayret, C.; Villesuzanne, A.; Pouchard, M.; Matar, S. *Int. J. Quantum Chem.* **2005**, *101*, 826.
(53) Frayret, C.; Villesuzanne, A.; Pouchard, M. *Chem. Mater.* **2005**, *17*, 6538.

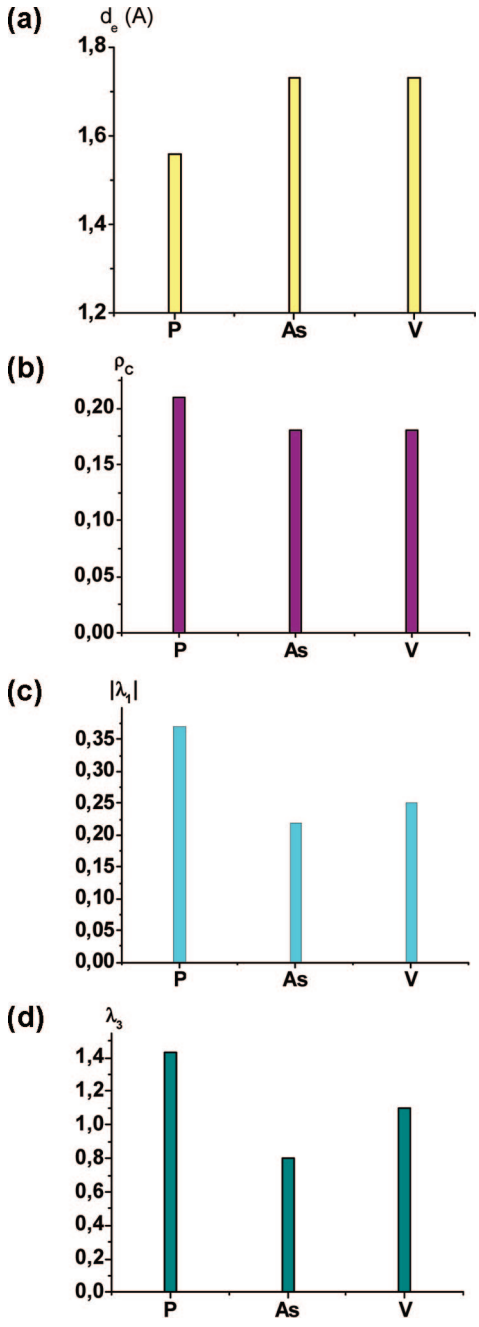

Figure 4. Li_3XO_4 (X = P, As, V) in the β-form: (a) bond length (l_e in Å), (b) electron density at the BCP (ρ_c in e Å^{-3}), and eigenvalues of Hessian at BCP (c) $|\lambda_1|$ and (d) λ_3 (in e Å^{-5}).

A way to catch such information is to consider the evolution of atomic basins within polyhedra, corresponding here to PO_4 and LiO_4 tetrahedra. Due to the local aspect of such an approach, volume evolution of atomic basins as compared with the one of the most stable form should be considered for each particular bond, and compared to the corresponding interatomic distance evolution. This description will be focused essentially on XO_4 tetrahedra, for which most of the evolution upon phase transition has been noticed (compared with LiO_4 tetrahedra). For Li_3PO_4, the phosphorus atom exhibits a decrease in volume by passing from the β- to the γ-form. Along the O_1-P bond, a decrease in oxygen volume is found, while an increase characterizes the O_3 volume evolution for the O_3-P bond. These results are consistent with the distance evolution during $\beta-\gamma$ inversion,

Table 9. Atomic Basin Volumes (Å^3) for the Two Polymorphs of Li_3XO_4 Calculated by the Bader AIM Approach within the Wien2k Implementation, Atomic Volume, and Interatomic Distances Evolutions with Respect to the Most Stable Phase (%) for the XO_4 Polyhedron

		V (Å^3)			
X		β	γ	$\Delta V/V_\beta$ (%)	Δd(X−O)/d_β (%)
P	P	3.103	2.961	−4.58	
	Li1	3.116	3.201	+2.73	
	Li2	3.317	3.179	−4.16	
	O1	17.761	16.983	−4.38	−0.38
	O2	17.242	18.932	+9.80	0
	O3	14.542	16.667	+14.61	+0.19
As	As	8.334	8.072	−3.14	
	Li1	3.220	3.253	+1.02	
	Li2	3.339	3.261	−2.34	
	O1	17.856	17.997	+0.79	−0.12
	O2	17.919	17.929	+0.056	−0.35
	O3	16.839	17.005	+0.99	+0.23
V	V	7.864	8.491	+7.97	
	Li1	3.218	3.226	+0.25	
	Li2	3.332	3.812	+14.41	
	O1	18.527	17.832	−3.75	−0.17
	O2	18.116	17.185	−5.14	−0.35
	O3	15.135	19.467	+28.62	+0.52

which are shortened and elongated, respectively (Figure 6a). On the other hand, while O_2-P bond does not undergo any change in distance, the O_2 volume is markedly enhanced ($\Delta V/V_\beta = +9.80\%$). This constitutes a local zone of electron cloud interpenetration and generates some strain within the PO_4 tetrahedron for the γ-form, which does not exist for the most stable phase. Concerning the orthoarsenate, all the oxygen ions tend to slightly increase their volume while the atomic basin for As is diminished during $\beta \rightarrow \gamma$ inversion. For both O_1-As and O_2-As bonds, the diminished interatomic distance associated with the volume increase of oxygen should result in some higher strain in the γ-form as compared with the β one (Figure 6b). Indeed, though the increase in oxygen volume is low as compared with the one encountered

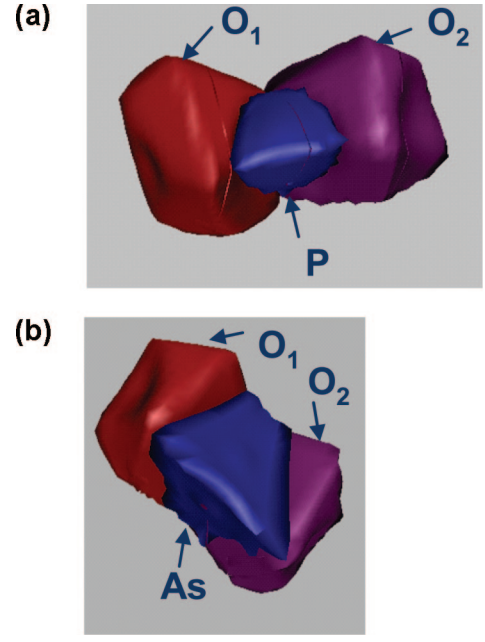

Figure 5. Atomic envelopes obtained by the topological analysis of the calculated electron density (rendered with GEOMVIEW): (a) Li_3PO_4 [phosphorus (blue), oxygen O_1 (red) and oxygen O_2 (purple) atoms] and (b) Li_3AsO_4 [arsenium (blue), oxygen O_1 (red) and oxygen O_2 (purple) atoms].

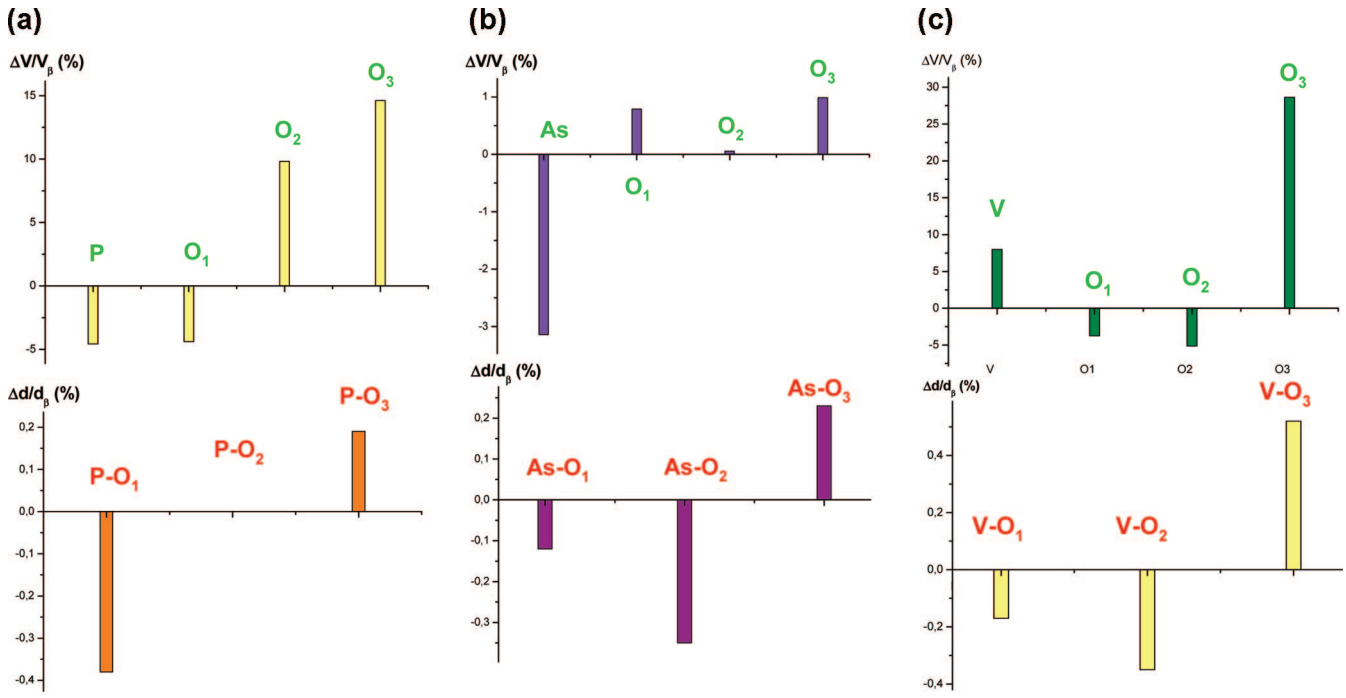

Figure 6. Relative evolution of atomic basin volumes during phase transition, $\Delta V/V_\beta$ (in %), and concomitant relative evolution in X−O distances, $\Delta d/d_\beta$ (in %): (a) Li_3PO_4, (b) Li_3AsO_4, and (c) Li_3VO_4.

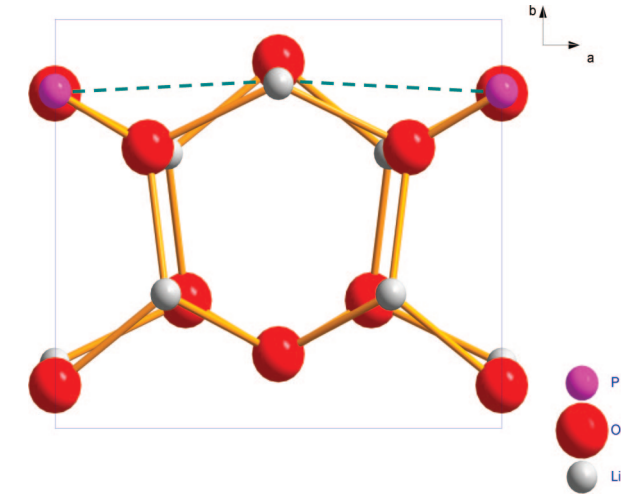

Figure 7. Electrostatic interactions within the *ab* plane of the β-polymorph (destabilizing interactions due to X···Li···X "alignments" are represented with a dotted line).

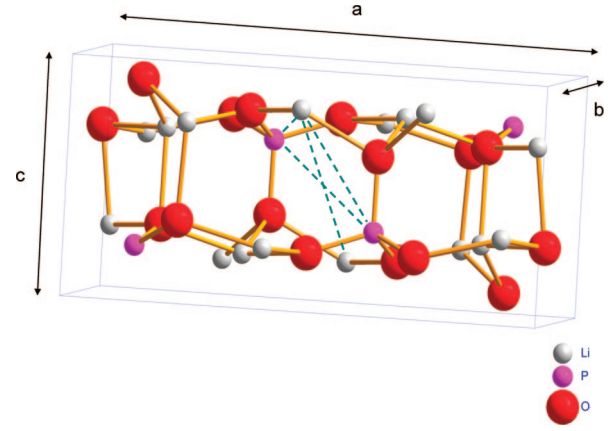

Figure 8. Electrostatic interactions in the γ-polymorph (destabilizing X···Li, Li···Li or X···X interactions are represented by dotted lines).

for the phosphate material, the distance decrease is quite significant and should generate much stronger strain within the polyhedra. Moreover, the size of the arsenic atom is also less diminished than that of the phosphorus one, and we observe opposite trends in distance and atomic volume evolution, whereas for Li_3PO_4 concomitant absence of change in distance and atomic volume increase were noticed, which is less penalizing. For the lithium orthovanadate, we observe that decreased (for O_1, O_2) or increased oxygen volumes (for O_3) match the evolution of V−O distances (shortening for V−O_1 and V−O_2/elongation for V−O_3). The strong volume augmentation of O_3 is consistent with the very high elongation of the V−O_3 bond (Figure 6c). However, the very strong increase of vanadium volume during $\beta \rightarrow \gamma$ inversion should counteract these effects and generate some strain within the tetrahedron. Apart from this trend concerning the VO_4 tetrahedron, we should mention that another enhancement of the strain component in the γ-form originates from the $Li(2)O_4$ tetrahedron, for which a slight diminishing of the Li(2)−O_3 distance is evidenced while both O_3 and Li(2) are characterized by atomic volume augmentation. Therefore, we can consider that due to these two components of mean magnitude, strain generated in the γ-form for Li_3VO_4 lies in between those of Li_3PO_4 (lowest strain) and Li_3VO_4 (highest strain).

As a whole, it appears that the lower stability of the γ-form as compared with the β-polymorph might, at least partly, originate from the higher strain within XO_4 tetrahedron, which is systematically encountered due to mismatch between atomic volume size and bond distance evolution. Furthermore, from the differences in discrepancy between volume and interatomic distance evolutions among Li_3PO_4, Li_3AsO_4, and Li_3VO_4, we expect higher strain for the γ-form in the rank: As $\gg$ V > P.

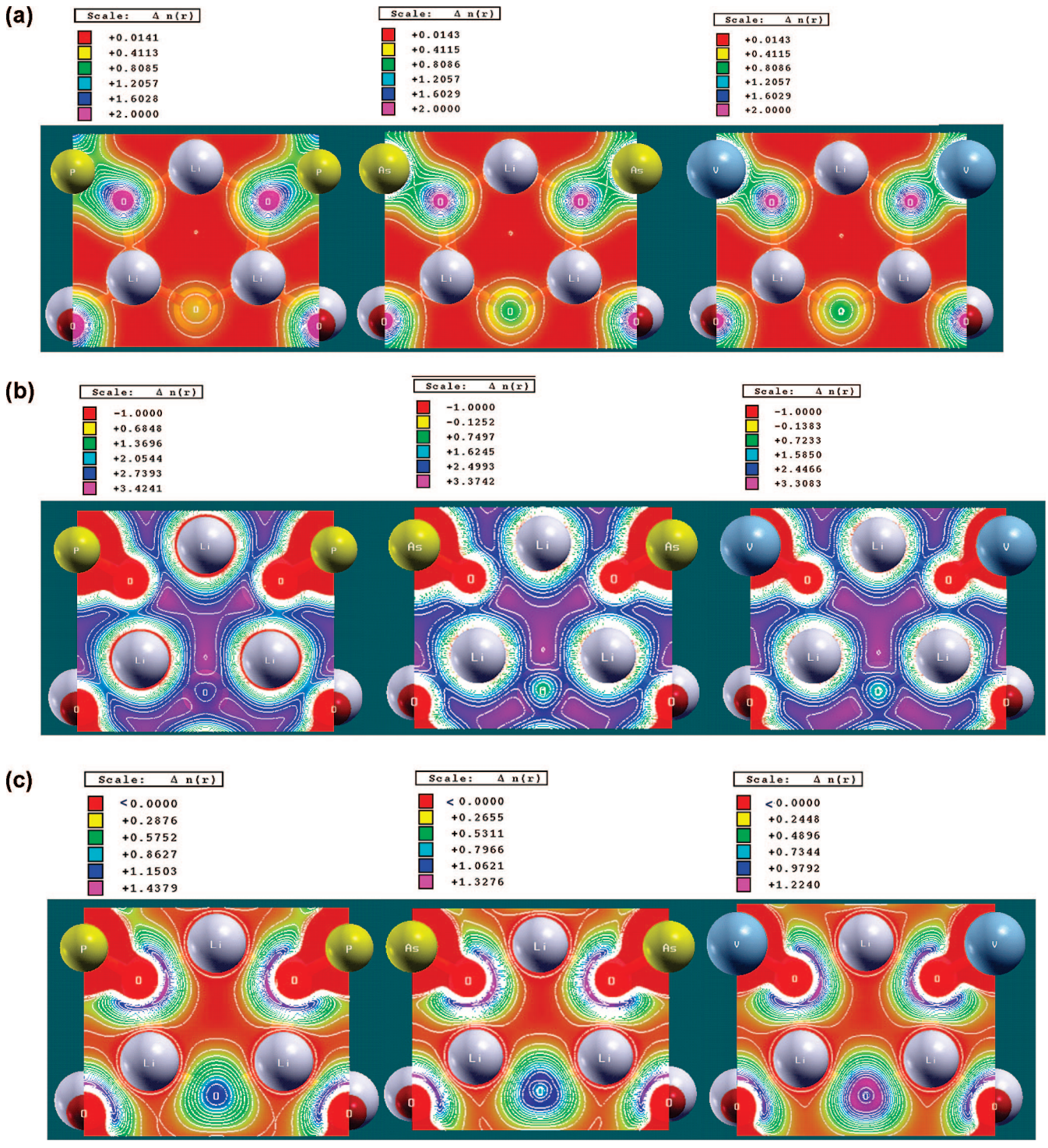

Figure 9. (a) Valence electron density maps, (b) Coulomb potential maps, and (c) energy density maps of the β-polymorph in Li_3XO_4 (from left to right: X = P, As, V).

8. Electrostatic Interactions

Apart from the aforementioned aspects, we should note that charges have a great impact not only on the chemical bonding nature (at least from a qualitative viewpoint as previously discussed) but also on electrostatic interactions within the crystal, which also predominantly play a role in phase stability for iono-covalent crystals.

Concerning electrostatic interactions in the β-form, one can observe that X···Li···X "alignments" are built up with alternant, slightly shifted O atoms (Figure 7). Therefore, screening of the repulsive cation interactions by the oxygen ions does occur. In the γ-phase, destabilizing interactions between cations are of X···Li, X···X and Li···Li type (Figure 8).

We can now investigate the possible connection between electrostatic interactions and the total energy differences between polymorphs in orthosalts. This analysis is based on the explicit calculation of attractive and repulsive electrostatic energy parts and the accurate examination of different maps,

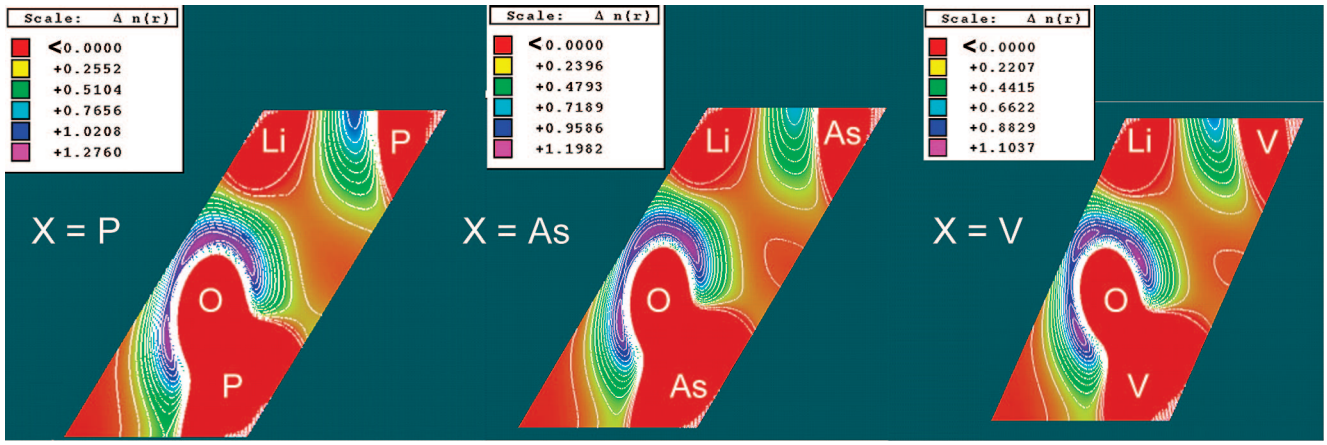

Figure 10. Energy density maps of the γ-polymorph in Li_3XO_4 (from left to right: X = P, As, V).

Table 10. Calculated Charges on P, As, V, and Li (only for the β-form) and Corresponding Repulsive Pair Electrostatic Interaction Component (ratio qq'/r in e^2/Å) in the Two Orthosalt Polymorphs

	β-form			γ-form		
	P···Li	As···Li	V···Li	P···P	As···As	V···V
q	+3.82	+2.73	+2.16	+3.82	+2.73	+2.16
q'	+0.89	+0.89	+0.89	+0.89	+0.89	+0.89
r	3.09	3.18	3.19	4.11	4.19	4.18
qq'/r	1.10	0.76	0.60	0.83	0.58	0.60

Table 11. Calculated Charges on P, As, V, and O and Corresponding Attractive Pair Electrostatic Interaction Component (ratio qq'/r in e^2/Å) in the β-Phase

	P···O	As···O	V···O
q	+3.82	+2.73	+2.16
q'	−1.62	−1.35	−1.20
r	1.56	1.73	1.74
qq'/r	−3.97	−2.13	−1.49

including valence electron density, Coulomb potential maps, and energy density maps. The last concept, corresponding to the product of a valence electron map and a Coulomb potential map has been developed previously and has proven to be an efficient tool in the field of atomic scale diffusion.[54−56] Table 10 displays the repulsive electrostatic energy component for the different cations involved in both β- and γ-phases. Attractive electrostatic interaction between lithium and X for the β-form are summarized in Table 11. Parts a, b, and c of Figure 9 display, respectively, the valence electron density, the Coulomb potential, and the energy density maps, for the *ab* plane, in the β-phase. This plane contains two X and three Li ions, and oxygen atoms in the vicinity of atoms contained within the plane are viewed thanks to the transparency of the plane. Figure 10 corresponds to the energy density map of the γ-phase within a plane containing two X and one Li ion (an O atom is seen in transparency).

For the β-phase, the repulsive part due to X···Li interactions is greater in Li_3PO_4 than in Li_3AsO_4, and that of arsenate also encompasses the one of vanadate. However, we observe that screening of cations by oxygen in the β-form is clearly more important for P than for As due to both the higher charge of P and O and to the lower P···O distance. Similarly, we observe, on the same grounds, that the attractive part between As and Li is prevailing over that characterizing V···Li interaction. As a whole, we can thus consider that, among the different interactions, there is clearly a competition between attractive and repulsive energy components that make difficult the ranking of the different orthosalts in terms of resultant electrostatic interactions. This is why it is crucial to get a picture of the extent of the resulting electrostatic interactions both spatially and quantitatively. Such information is provided by considering the electrostatic energy maps, along with valence electron density and Coulomb potential maps from which they are built, since they also afford some interesting features.

First of all, valence electron density maps illustrate well chemical bonding results described in the previous section, with an almost ionic bonding between lithium and oxygen ions (the electron density being confined on lithium ion), and a quite pronounced covalent character of X−O bonds, for which high expansion of electron density along the interatomic direction is evidenced.

Such a bonding scheme strongly enhances the region in space for which high electron density is present and is therefore unfavorable from the viewpoint of the electrostatic interactions by extending electrons in the vicinity of the lithium ions. Coulomb potential maps indicate both a negative potential between X and O resulting from the electrostatic attraction and repulsive (positive) potential throughout the plane containing the different cations. By multiplying Coulomb potential and valence electron density maps, the area of negative potential is preserved, generating a negative stabilizing interaction between O and X ion. From

(54) Frayret, C.; Villesuzanne, A.; Pouchard, M. In *Computational Modeling and Simulation of Materials III: Proceedings of the 3rd International Conference on "Computational Modeling and Simulation of Materials"*; Techna-Group Series Advances in Science and Technology, 42−46; May 30−June 4, 2004, Acireale, Sicily; Part A, p 797.
(55) Frayret, C. Ph.D. thesis, University of Sciences and Technologies: Bordeaux, 2004.
(56) Lontsi-Fomena, M.; Villesuzanne, A.; Doumerc, J. P.; Frayret, C.; Pouchard, M. *Comput. Mater. Sci.* **2008**, *44*, 53.

the energy density maps, we also observe that highly positive (and thus unfavorable) regions of energy are generated in the area where both the Coulomb potential is positive and the electron density is high. In fact, it is relevant to note that even the electron density of oxygen ion, lying within the global positive electrostatic potential generated by the neighboring cations, strongly participates in the occurrence of a positive energy density component.

Using these maps, the ranking in terms of global resultant electrostatic interactions is unambiguously evidenced, with positive electrostatic energy density rising in the order V, As, and P. From the highest positive energy density values (represented in pink in the Figure 9c) it is straightforward to see that the relative energy difference between V and As (8%) is of the same extent as the one characterizing the change from As to P (~8%). Therefore, in terms of incidence of the electrostatic component on the stability, the β-phase is expected to be the most stable for vanadate and the less stable for phosphate material, the arsenate lying in between.

In the γ-form, the repulsive component between X ions is enhanced by a factor of nearly 1.3 by passing from Li_3VO_4 to Li_3AsO_4 and then once more from Li_3PO_4 to Li_3VO_4. This tends to induce a greater destabilization of the γ-phase in the rising order V, As, P. The Li···Li interactions in this phase are very similar among the three orthosalts and are thus not listed here while X···Li interactions are probed directly from the energy density maps. In fact, similarly to the β-phase, one can observe that one of the surrounding oxygen atoms has an effect of screening, too. As previously mentioned, a higher stability is found in the order V, As, P (Figure 10) and the relative energy difference between V and As (8.6%) is roughly of the same extent as the one characterizing the passage from As to P (7%). Moreover, the involved values are somewhat equivalent to the ones characterizing the β-phase.

As a result, it clearly appears that long-range electrostatic effects are in fact a delicate balance between attractive and repulsive components for both polymorphs. The same ranking evidenced for both forms (β and γ) among the Li_3XO_4 series (rising stability in the order P, As, V) does not afford any distinction between the different cations. Therefore, we suggest that electrostatic interactions do not play a significant role in the difference in total energies, ΔE, among X = P, As, and V.

9. Rationalization of the Polymorphism Features

From the previous detailed study of chemical bonding, electrostatic interactions, and elastic strain features, it clearly appears that effects underlying phase stability within the family of lithium orthosalts [Li_3XO_4 (X = P, As, V)] can be divided into two main classes: (i) effects acting only on the ranking in stability according to the nature of X in the materials and (ii) effects having an incidence on the relative stability of the two polymorphs within a given class of compound (i.e., for one particular X).

Concerning the first kind of effects, we have seen that higher stability is found in the order V, As, P from the electrostatic interactions viewpoint, while higher stability for the phosphate is afforded according to bonding features, with much weaker V−O or As−O bonds. These trends, counteracting each other, tend to reduce the gap in phase stability as a function of the nature of X.

Differences in stability between the two polymorphs are most probably due to the elastic strain resulting from mismatch between atomic volume and interatomic distance evolutions within a polyhedron. A higher strain is expected for the γ-form in the rank As $\gg$ V > P. Therefore, low, mean, and high differences in energy are respectively expected for Li_3PO_4, Li_3VO_4, and Li_3AsO_4. For this last material, another destabilization of the γ-phase with respect to the β one comes from the loss in ionic character of one of the Li−O bond. From these phenomena, the rationalization of the polymorphism distinction among the Li_3XO_4 (X = P, As, V) family is possible, since the difference in energy between β- and γ-polymorphs is rising in the order orthophosphate, vanadate, and arsenate. These results are in agreement with the higher temperatures required for the vanadate or arsenate for phase transformation.

Apart from this first classification, we should note that, in fact, chemical bonding features can also have an indirect incidence on the phase transition characteristics. Indeed, the more ionic bonding character of the phosphate can be related not only to higher bond strength but also to higher cation mobility. From this viewpoint, since the high $\rightarrow$ low phase transformation originates from reorganization of cations within tetrahedral sites (half of the cations jumping from one set of the tetrahedral sites to another), it should become progressively easier to break bonds in the order V−O (or As−O), P−O; cations' mobility should decrease in the order P, V (or As). All these effects provide further explanations on both (i) the lowest temperature required for the $\beta \rightarrow \gamma$ transformation in Li_3PO_4 (around 400−600 °C against ~750 °C for Li_3VO_4 and Li_3AsO_4), which might be due also to better ionic diffusivity of phosphate cations as compared with that of V or As within the same framework, and (ii) the much faster transformation for Li_3VO_4 and Li_3AsO_4, which could be related to easier breaking of initial bonds within VO_4 or AsO_4 tetrahedra in comparison with PO_4 ones.

10. Conclusion

Structural, electronic, and topological properties of fully optimized lithium orthosalt polymorphs [Li_3XO_4 (X = P, As, V)] were characterized by DFT calculations and electron density partition. Our objectives in this study were first to identify the relative stability of the two polymorphs within the series and then to determine whether it is ascribable to some peculiar features at the atomic scale. The following main conclusions can be drawn.

(1) For all the studied lithium orthosalts, it is found that the β-polymorph is the most stable one, agreeing well with experimental results. The energy difference between β- and γ-phases increases by passing from P (~0.01 eV/fu) to V and As, with double (~0.02 eV/fu) and triple (~0.03 eV/fu) order of magnitude in stability found for the β-polymorph of the two last compounds, respectively.

(2) Our population analysis first provides insight into the relative ionicity of different materials and tends to indicate

that no difference is found between the two polymorphs. From atomic charges and band gaps values, it appears that ionicity strongly decreases from the phosphate to the arsenate or vanadate.

(3) The bond critical points analysis affords deeper and very precise insight into the differences in chemical bonding nature between the various lithium orthosalts. A weaker V−O or As−O bonding relative to P−O bonding in both β- and γ-forms is evidenced and Li_3AsO_4 is the only compound for which a distinction is found between the two polymorphs, with one Li−O bond in the γ-form losing its ionic character as compared with the situation in the β-form.

(4) The electrostatic component of the energy was characterized both in terms of attractive and repulsive pair interactions between ions and energy density maps, allowing us to give a detailed picture of the area of resultant positive (destabilizing) and negative (stabilizing) contribution to the energy.

(5) A quite significant evolution in atomic volumes is found by passing from one polymorph to another. The lower stability of the γ-form as compared with the β-polymorph originates, at least partly, from the higher strain within XO_4 tetrahedron, which is systematically encountered due to mismatch between atomic volume size and bond distance evolutions.

(6) Some rationalization of the polymorphism features is possible: it is found that the ranking in energy differences between β- and γ-forms according to the nature of X can be closely related to the differences in constraints augmentation within XO_4 tetrahedron during phase transformation and to the loss in one part of the stability component for the γ-form of Li_3AsO_4 (from the chemical bonding viewpoint). Temperatures of phase transitions, already in perfect match with these energy differences, can also be explained through the higher ionic bonding character of P−O in comparison with V−O or As−O bonds, if one considers migration of cations occurring during the phase transformation.

Such a fruitful approach could open the way to other investigations of phase transition and polymorphism in relation with phase structural stability, which is known to be required especially for reversibility of insertion/extraction in lithium battery compounds. In our group, we are currently applying these concepts to the Li_2MSiO_4 family.

Acknowledgment. We acknowledge the computational facilities provided by the computer center of the University Bordeaux 1 within the M3PEC (http://www.m3pec.u-bordeaux1.fr) intensive calculations project partly financed by the Conseil Régional d'Aquitaine. The support from the European Network of Excellence "ALISTORE" is acknowledged. Gérard Quoirin is also acknowledged for discussions.

CM803429S